# Supporting Information

## Drake et al. 10.1073/pnas.1319948110

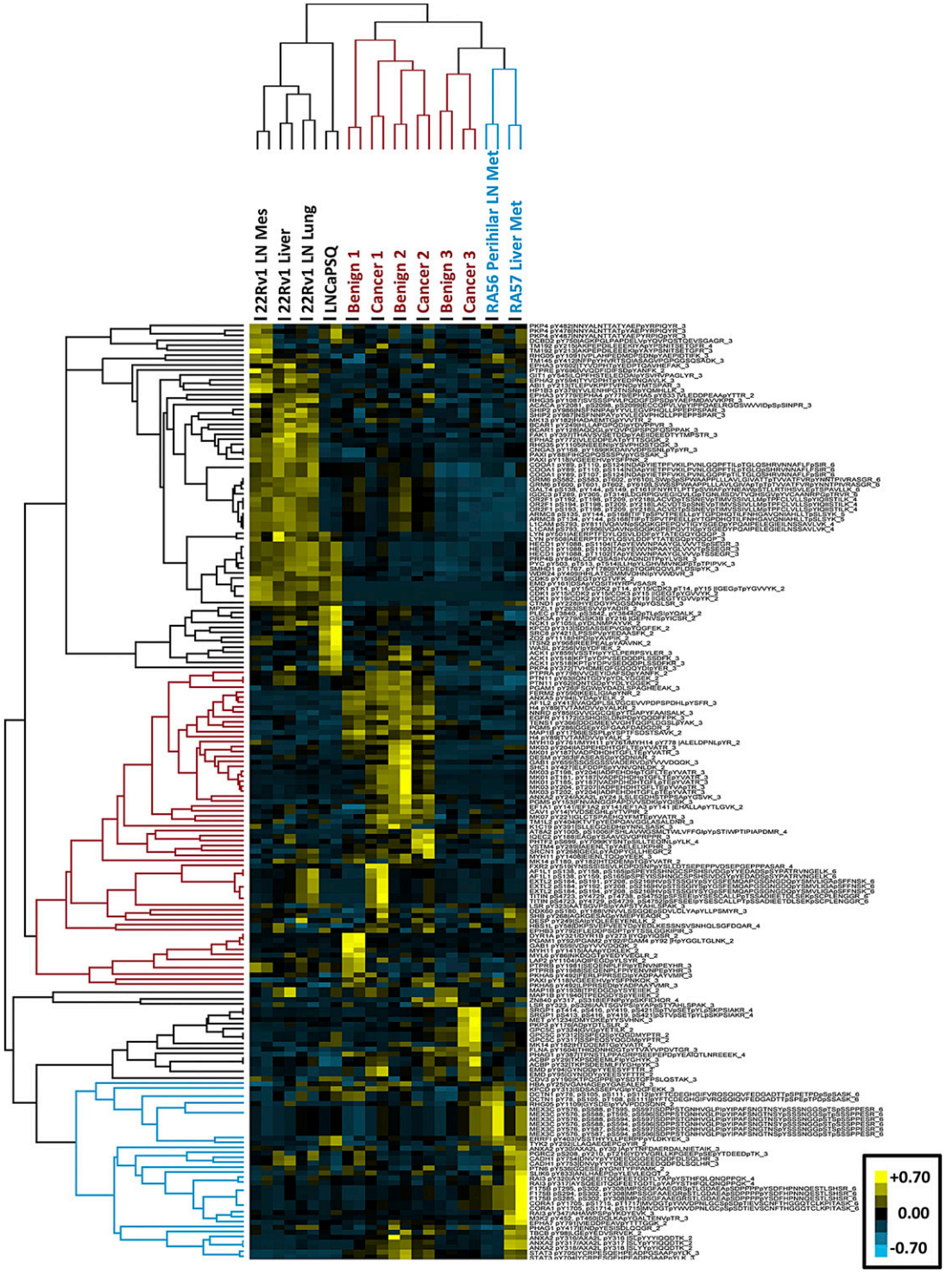


**Fig. S1.** Phosphoproteomic analysis exhibits distinct clusters of phosphorylation between the cell line-derived xenografts and primary prostate tissues. Unsupervised hierarchical clustering does not group cell line-derived metastatic xenograft tumors with either organ confined or metastatic castration-resistant prostate cancer (CRPC). In addition, treatment-naïve patient-matched benign and cancerous prostates display indistinguishable phosphopeptide signatures. The phosphoprofiling heatmap from Fig. 2*A* with the protein and residue identities of the phosphorylation events are listed. For all heatmaps, the labels are as follows: UniProt ID, phosphosite residue number, phosphopeptide (charge state of mass spectrometry ion). If the phosphopeptide has multiple identities, a slash separates each protein and phosphorylation residue number. The vertical line separates the proteins from the phospho-peptide. Yellow, hyperphosphorylation; blue, hypophosphorylation.

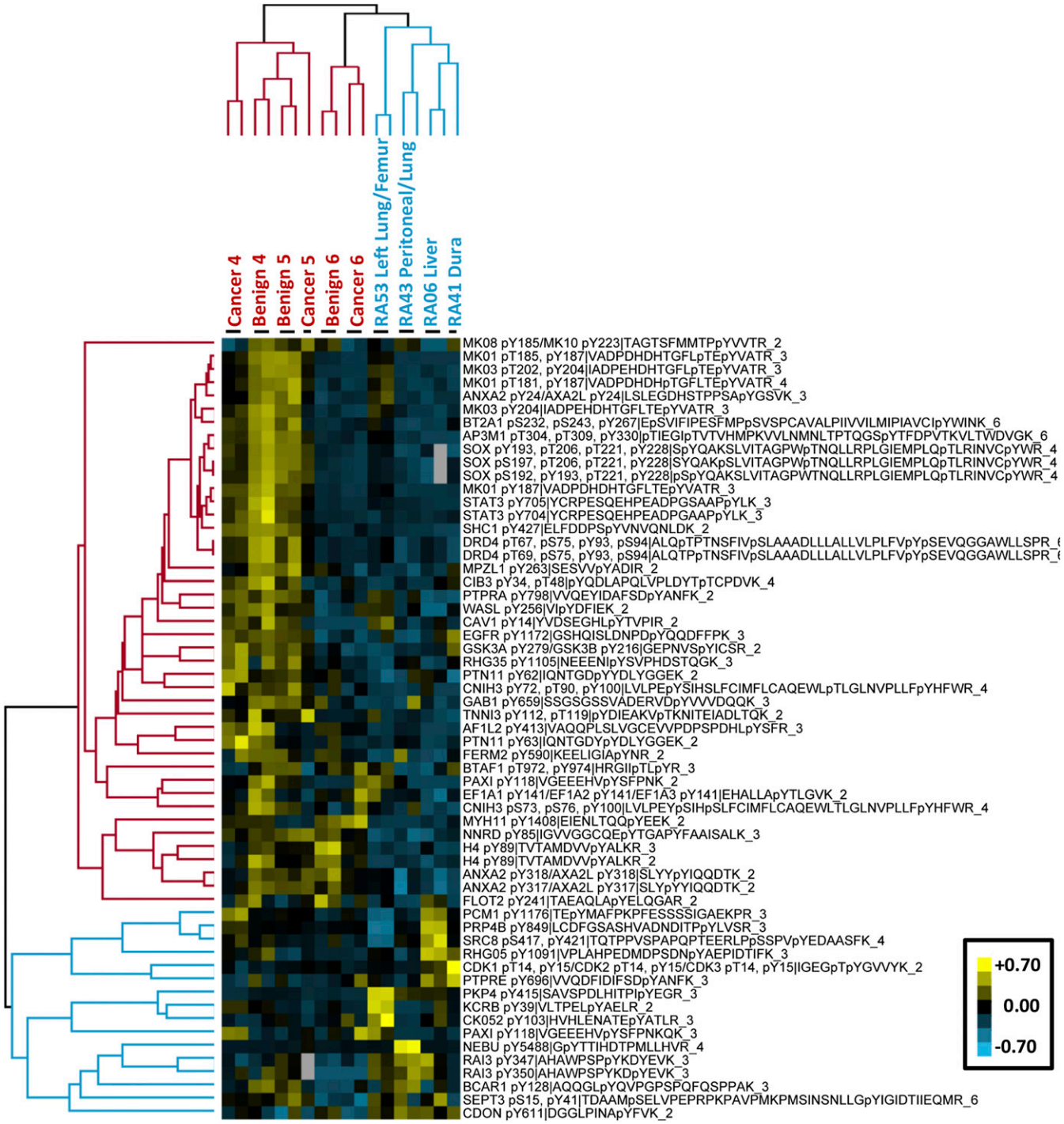


**Fig. S2.** Phosphoproteomic analysis exhibits distinct clusters of phosphorylation between treatment-naïve prostate cancer and metastatic CRPC. Unsupervised hierarchical clustering does not group organ-confined prostate benign or cancerous prostates with metastatic CRPC. Also, treatment-naïve patient-matched benign and cancerous prostates display indistinguishable phosphopeptide signatures. The phosphoprofiling heatmap from batch 2 with the protein and residue identities of the phosphorylation events are listed. For all heatmaps, the labels are as follows: UniProt ID, phosphosite residue number, phosphopeptide (charge state of mass spectrometry ion). If the phosphopeptide has multiple identities, a slash separates each protein and phosphorylation residue number. The vertical line separates the proteins from the phosphopeptide. Yellow, hyperphosphorylation; blue, hypophosphorylation.

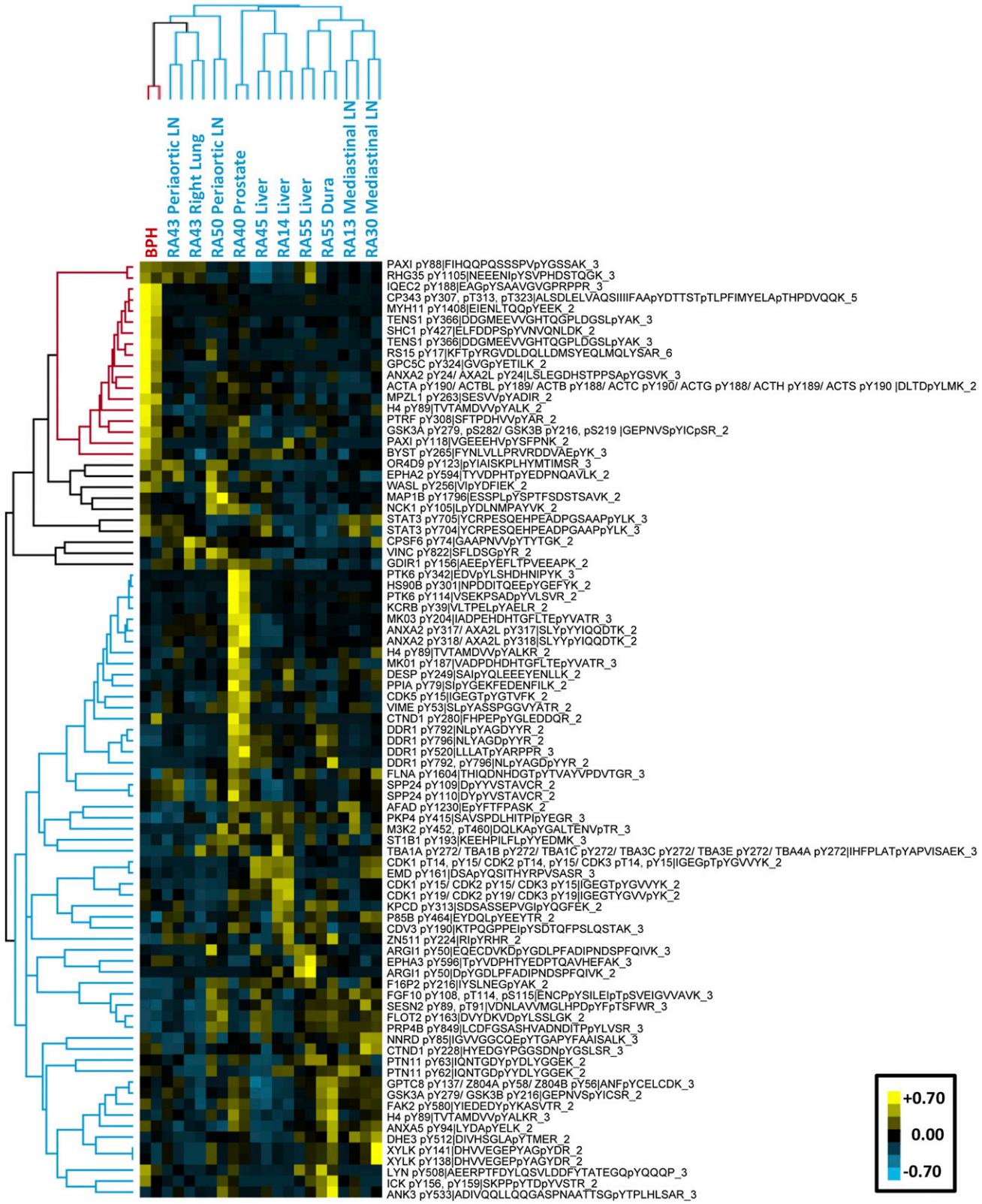


**Fig. S3.** Phosphoproteomic analysis exhibits both patient-specific and metastatic site-specific patterns of tyrosine kinase activation in metastatic CRPC. Unsupervised hierarchical clustering groups by organ site of metastases as well as by intrapatient metastatic lesions. Benign prostatic hyperplasia (BPH) was used as the treatment-naïve tissue for comparison. The phosphoprofiling heatmap from Fig. 2*B* with the protein and residue identities of the phosphorylation events is listed. For all heatmaps, the labels are as follows: UniProt ID, phosphosite residue number, phosphopeptide (charge state of mass spectrometry ion). If the phosphopeptide has multiple identities, a slash separates each protein and phosphorylation residue number. The vertical line separates the proteins from the phosphopeptide. Yellow, hyperphosphorylation; blue, hypophosphorylation.

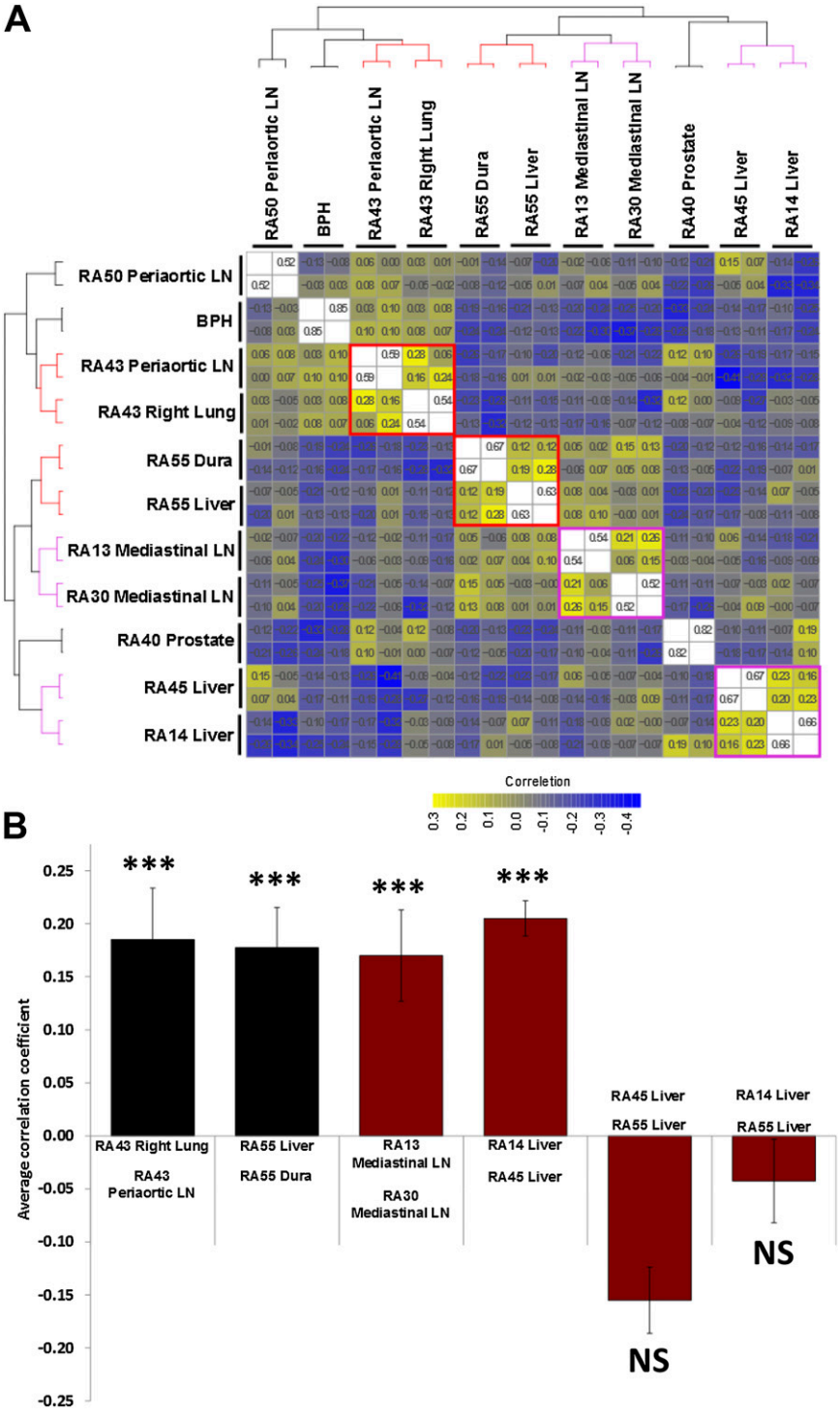


**Fig. S4.** Phosphoproteomic data reveal high levels of intrapatient similarity and occasional high levels of intraanatomical site similarity. (*A*) Pairwise Pearson correlation coefficients for each phosphotyrosine sample (including technical duplicates) were calculated and then clustered. The correlation coefficients are superimposed on each color-coded square. The correlation coefficients on the diagonal and the correlation coefficients for technical replicates were omitted from the color scale. (*B*) Pairwise correlation coefficients, excluding technical replicates, were averaged, and the statistical significance against the null hypothesis that the correlation was not greater than zero was calculated. Error bars are the SE. ***$P < 0.001$; NS, not significant.

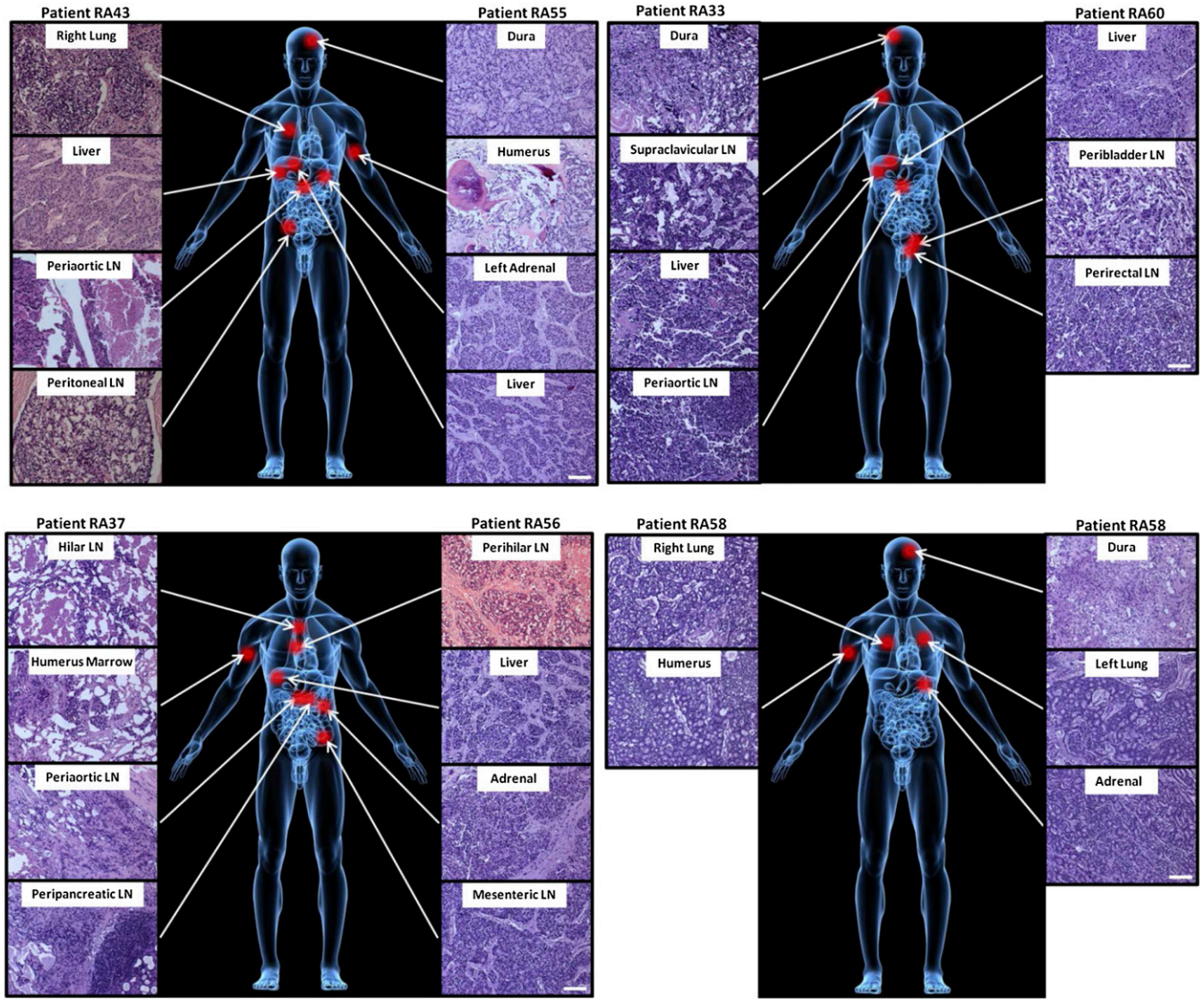


**Fig. S5.** Location and histological characterization of seven patients with anatomically distinct metastatic CRPC lesions. Seven separate patients' metastatic lesions are depicted with representative histology. These samples were used for western blot and phospho–receptor tyrosine kinase (RTK) and phosphokinase arrays. Red dots indicate the approximate location of the metastatic lesions analyzed. Tissues with greater than 50% tumor content were evaluated. (Scale bar, 50 μm.)

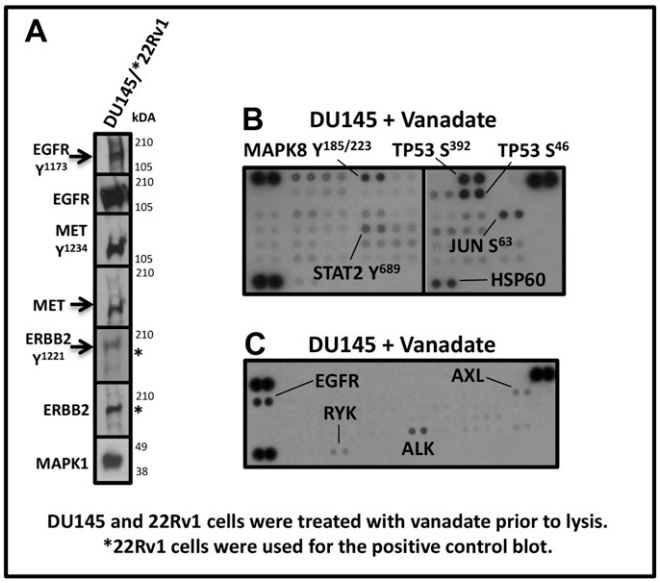


**Fig. S6.** Evaluation of RTK epidermal growth factor receptor (EGFR), erythroblastic leukemia viral oncogene homolog 2 (ERBB2 or HER2/neu), and hepatocyte growth factor receptor (HGFR or MET) and phospho-kinase and phospho-RTK arrays using positive control prostate cancer cell lines. Western blot analyses from DU145 or 22Rv1 cells treated with the phosphatase inhibitor, vanadate, were evaluated for the activated states of the RTKs EGFR, ERBB2, and MET (*A*); phosphokinase (*B*); or phospho-RTK arrays (*C*). DU145 or 22Rv1 (indicated by an asterisk next to the blot) cells were used as positive controls.

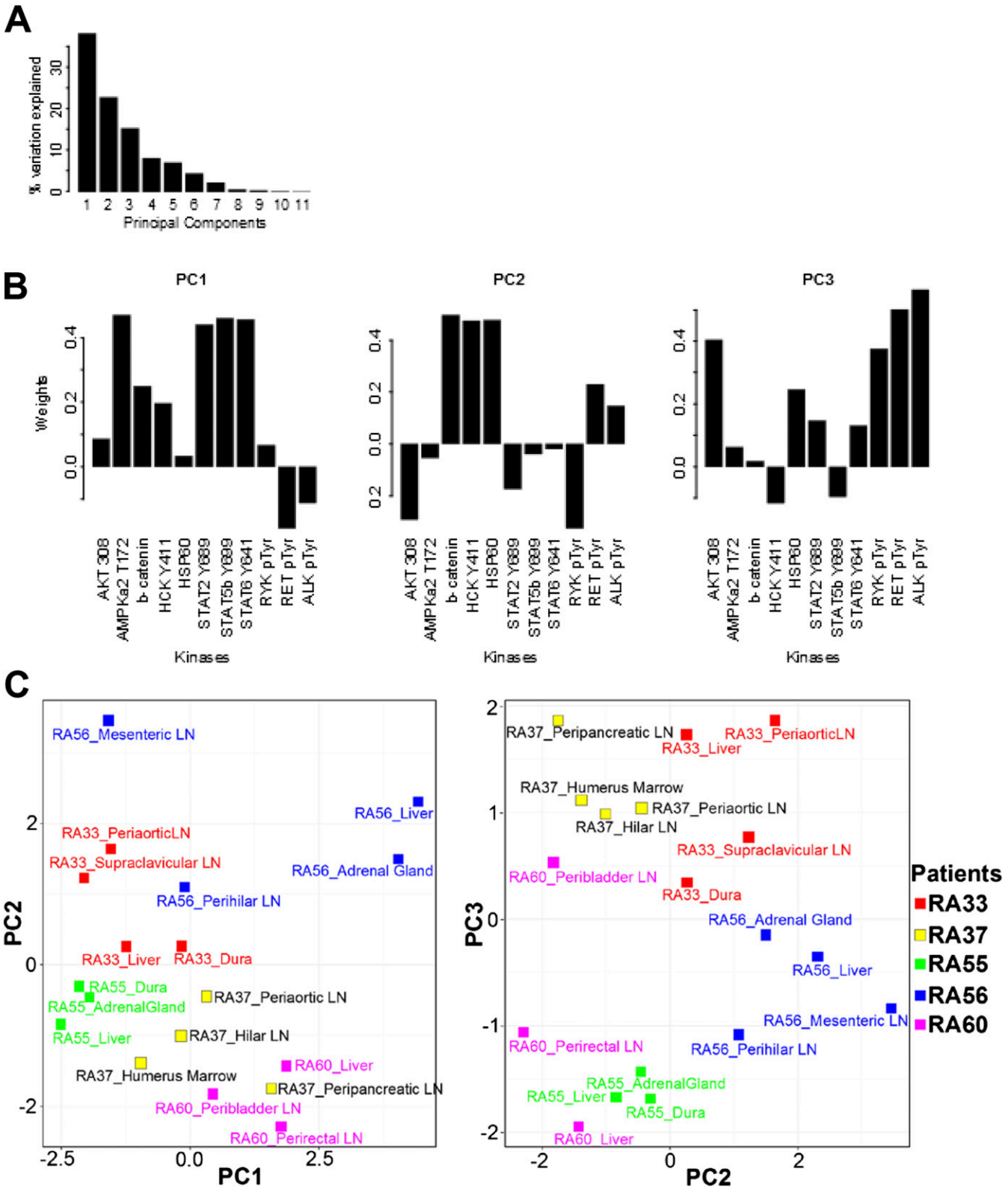


**Fig. S7.** Principal component (PC) analysis of phosphokinase arrays. Data from CRPC metastatic samples analyzed by phosphokinase arrays were subjected to PC analysis. After removal of antibodies with negligible signal, 11 kinases remained: AKT $T^{308}$, protein kinase, AMP-activated, alpha 1 catalytic subunit (PRKAA1 or AMPKa) $T^{172}$, β-catenin, hemopoietic cell kinase (HCK) $Y^{411}$, STAT2 $Y^{689}$, STAT5b $Y^{699}$, STAT6 $Y^{641}$, receptor-like tyrosine kinase (RYK) phosphotyrosine, rearranged during transfection (RET) phosphotyrosine, and anaplastic lymphoma kinase (ALK) phosphotyrosine. (*A*) Schematic of the loadings vectors for the first three PCs. (*B*) The percentages listed for each PC indicated the amount of variance explained by that PC. (*C*) Plots of the PC analysis for all five patients analyzed demonstrate intrapatient kinase expression similarity and individual differences.

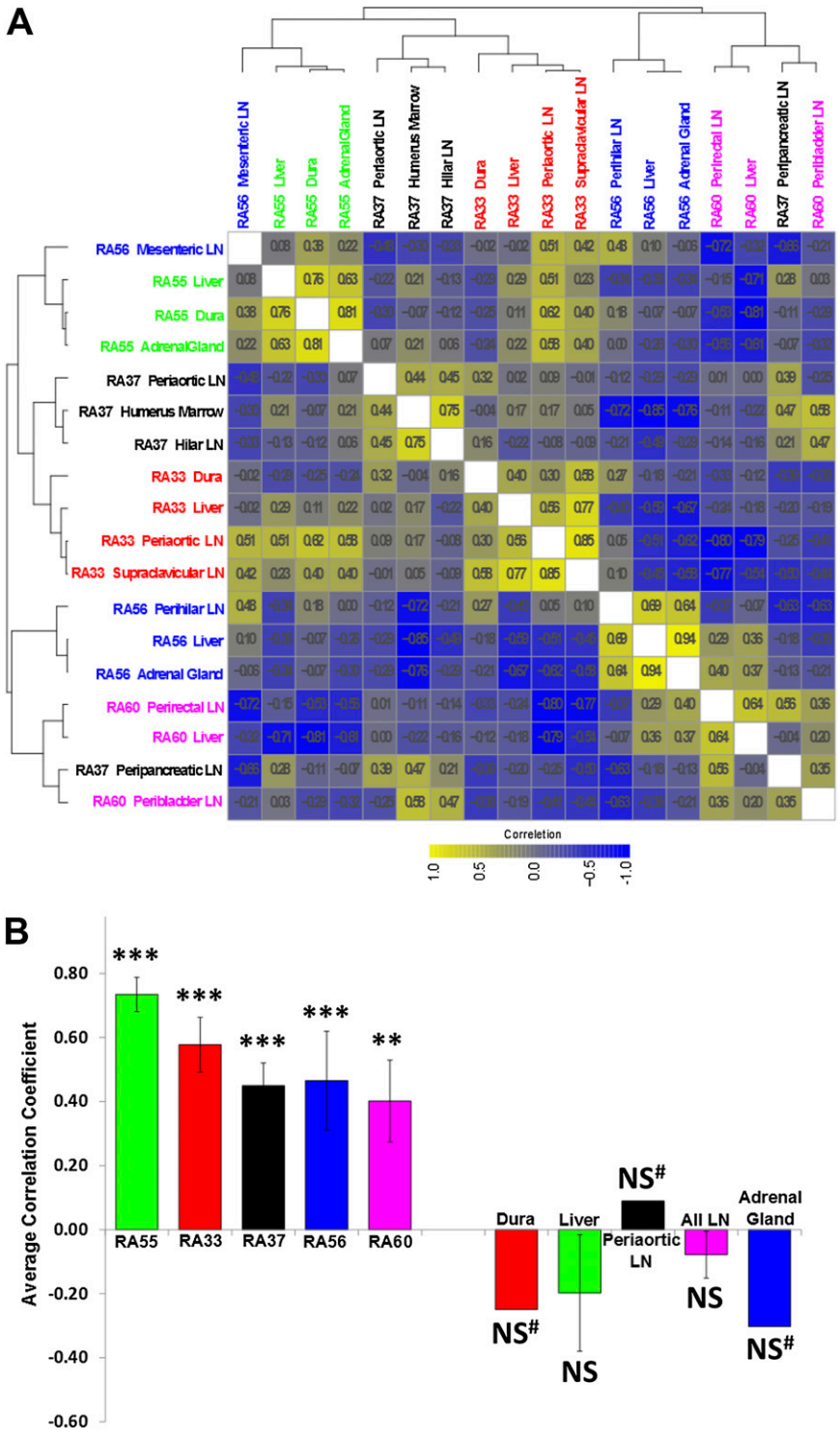


**Fig. S8.** Phosphokinase arrays demonstrate high levels of intrapatient but not interpatient similarity. (*A*) Pairwise Pearson correlation coefficients for each sample measured on the phosphokinase and phospho-RTK arrays were calculated and then clustered. The correlation coefficients are superimposed on each color-coded square. The correlation coefficients on the diagonal were omitted for readability. (*B*) Pairwise correlation coefficients were averaged, and the statistical significance against the null hypothesis that the correlation was not greater than zero was calculated. Error bars are the SE. Multiple *P* values were combined using Fisher's Method. ***$P < 0.001$, **$P < 0.01$; NS, not significant; #, single *P* value, not Fisher's combined.

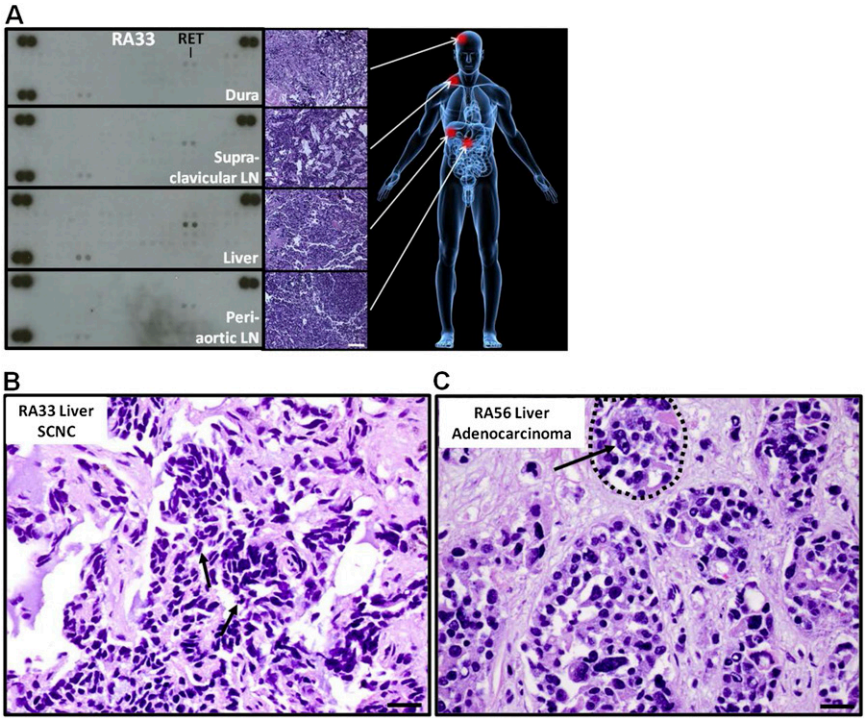


**Fig. S9.** Tyrosine phosphorylation of RTK RET in small cell neuroendocrine carcinoma (SCNC). (*A*) Analysis of patient RA33 using RTK arrays revealed the tyrosine phosphorylation of neuronal tyrosine kinase RET. (*B*) Metastatic tumor cells in this patient demonstrate typical nuclear morphology of SCNC including a darkly stained nucleus with a homogeneous chromatin pattern, high nuclear/cytoplasmice ratio, lack of nucleoli, and frequent mitotic figures (*B*, arrows). These characteristics are in sharp contrast to the nuclear morphology of adenocarcinoma tumor cells (*C*) that have open and vesicular chromatin patterns and prominent nuclei (*C*, arrow) and glandular formation (*C*, dashed circle). (Scale bar, 25 μm.)

## Other Supporting Information Files

Dataset S1 (XLSX)
Dataset S2 (XLSX)
Dataset S3 (XLSX)
Dataset S4 (XLSX)
Dataset S5 (XLSX)